New Astronomy 17 (2012) 542–551

Contents lists available at SciVerse ScienceDirect

New Astronomy

journal homepage: www.elsevier.com/locate/newast

A multiwavelength study of an M-class flare and the origin of an associated eruption from NOAA AR 11045

B.N. Dwivedi [a,*], Abhishek K. Srivastava [b], Mukul Kumar [a], Pankaj Kumar [c]

[a] Department of Applied Physics, Institute of Technology, Banaras Hindu University, Varanasi 221 005, India
[b] Aryabhatta Research Institute of Observational Sciences (ARIES), Nainital 263 129, India
[c] Korea Astronomy and Space Science Institute (KASI), Daejeon 305-348, Republic of Korea

ARTICLE INFO

Article history:
Received 28 March 2011
Received in revised form 11 October 2011
Accepted 19 October 2011
Available online 13 November 2011

Communicated by W. Soon

Keywords:
Corona
Solar flares
Reconnection
CME

ABSTRACT

In this paper, we study multiwavelength observations of an M6.4 flare in Active Region NOAA 11045 on 7 February 2010. The space- and ground-based observations from STEREO, SoHO/MDI, EIT, and Nobeyama Radioheliograph were used for the study. This active region rapidly appeared at the north-eastern limb with an unusual emergence of a magnetic field. We find a unique observational signature of the magnetic field configuration at the flare site. Our observations show a change from dipolar to quadrapolar topology. This change in the magnetic field configuration results in its complexity and a build-up of the flare energy. We did not find any signature of magnetic flux cancellation during this process. We interpret the change in the magnetic field configuration as a consequence of the flux emergence and photospheric flows that have opposite vortices around the pair of opposite polarity spots. The negative-polarity spot rotating counterclockwise breaks the positive-polarity spot into two parts. The STEREO-A 195 Å and STEREO-B 171 Å coronal images during the flare reveal that a twisted flux tube expands and erupts resulting in a coronal mass ejection (CME). The formation of co-spatial bipolar radio contours at the same location also reveals the ongoing reconnection process above the flare site and thus the acceleration of non-thermal particles. The reconnection may also be responsible for the detachment of a ring-shaped twisted flux tube that further causes a CME eruption with a maximum speed of 446 km/s in the outer corona.

© 2011 Elsevier B.V. All rights reserved.

1. Introduction

Small- and large-scale solar transient phenomena (e.g., surges/jets, spicules, anemone/penumbral jets, solar flares, CMEs, eruptive prominences, etc.) have been extensively studied. The multiwavelength observations of highly dynamical plasma processes in large- and small-scale transient/eruptive events as well as energetic particles in the Sun's atmosphere provide clues to understanding the hot plasma embedded in a complex magnetic field. Understanding the energy build-up/energy-release processes and plasma dynamics in the solar eruptive events are at the forefront of solar research. They have potential implications on the space weather in the ascending phase of current solar cycle 24. We have come a long way in understanding solar flares and CMEs since the advent of the space-based multiwavelength observations on board SOHO, STEREO, TRACE, Hinode and SDO in addition to high resolution ground-based observations. Moreover, space missions such as Wind, Advanced Composition Explorer (ACE), and Ulysses have provided complementary *in situ* information on interplanetary manifestations of CMEs associated with solar flares or those that are triggered independently. The Solar Terrestrial Relations Observatory (STEREO), Hinode, and Solar Dynamics Observatory (SDO) provide rich data sources both at higher resolution than previous observatories and at multiple temperatures to better understand the plasma dynamics as well as associated changes in the magnetic field topology of the flaring regions. STEREO also provides crucial information on the 3-D nature of CMEs and their source regions. Advances in observational techniques and equipment impose constraints on the theory of solar flares and CMEs.

Recently, Jain et al. (2010) have reported that the initiation and velocity of CMEs probably depend on the dominant process of the conversion of an active region's magnetic field energy into heating/accelerating the coronal plasma in the reconnected loops. These results show that a flare and associated CME are two components of one energy release system, which is probably the magnetic field free energy. Kumar et al. (2010a) have found a signature of CME eruption and triggering of an M-class flare in NOAA AR 10501 due to filament interaction leading to the release of magnetic energy in the lower solar atmosphere. Kumar et al. (2010b) have also found evidence of an M-class solar flare energy release due to loop–loop interactions in AR NOAA 10875. The instability in the

* Corresponding author.
E-mail address: bholadwivedi@gmail.com (B.N. Dwivedi).

1384-1076/$ - see front matter © 2011 Elsevier B.V. All rights reserved.
doi:10.1016/j.newast.2011.10.004

magnetic structures of the active regions may also cause an energy build-up and subsequent release in the form of solar flares and CMEs, either correlated with each other or independent (e.g., Foullon et al., 2011; Kumar et al., 2010c; Srivastava et al., 2010; Cho et al., 2009; Liu et al., 2008, and references cited there). Shen et al. (2011) have recently reported the dynamics of a filament from NOAA AR 11045 that failed to erupt several times, but finally erupted on February 8th, 2010, after being triggered by a C-class flare process which was associated with CMEs. They have attributed the eruption to the magnetic energy release resulting from the reconnection of erupting filaments with the ambient coronal magnetic field. Kumar et al. (2011) have also reported multiwavelength observations of a flux rope that failed to erupt from AR 11045 on February 12th, 2010 due to a remnant filament as well as the associated triggering of an M-class flare. In the present paper, we study multiwavelength observations of an M-class flare in the Active Region NOAA AR 11045 on February 7th, 2010. We also report a unique observational signature of the magnetic field configuration at the flare site showing a change from dipolar to quadrapolar topology. This change in the magnetic field configuration results in its complexity and the build-up of solar flare energy as well as the associated eruption. In Section 2, we present the multiwavelength observations of the solar flare and CMEs. We discuss the results in the last section.

2. Multiwavelength observations of NOAA AR 11045 on 7 February 2010

The active region, NOAA 11045, was very dynamic and produced more than 40 flares above C-class between February 6th and 14th, 2010 (Xu et al., 2010). This active region started decaying on February 12th, 2010 near the western limb, showing a magnetic configuration. However, this active region also showed a large flux emergence during its journey over the solar disk, with a large, rapid event near the northeast limb on 6 February 2010. Fig. 1 shows data taken on 7 February 2010 of an M6.4 flare's phases in soft X-ray (GOES) and various radio frequencies (RSTN station), which are at the two extreme ends of the electromagnetic spectrum observed in typical flare processes. According to GOES soft X-ray flux measurements (top-panel), this M6.4 flare started at ~02:24 UT, reached a maximum at ~02:34 UT, and ended at ~03:24 UT with its long-duration decay phase. However, as per the EIS flare catalog, the flare starts at 02:20 UT, maximises at 2:34 UT, and decays at 02:39 UT (cf., http://msslxr.mssl.ucl.ac.uk:8080/SolarB/eisflare2010.jsp). The flare rose gradually with the activation of the complexity in the photospheric magnetic field at the flare site followed by a mass eruption and corresponding slow CME in the outer corona. In the following subsections, we describe the multiwavelength observations of an M-class flare and its associated eruptions.

2.1. STEREO-A and B He II 304 Å chromospheric observations

Figs. 2 and 3 are the selected typical sequence of EUV (304 Å) STEREO-A and B/SECCHI images. This filter reveals ionized helium (He II) at the formation temperature of $\sim 10^5$ K. This filter can observe prominences and filaments above the Sun's surface in its lower atmosphere. The STEREO He II 304 Å images also reveal the upper chromosphere at higher temperatures. The NOAA AR 11045 was located near the northeast limb in the field of view of STEREO-A SECCHI. However, it was observed near the northwest limb by STEREO-B. This is mainly due to an acute angle separation between them during observations of the particular active region. Therefore, observations of the same active region from different angles provide opportunities to analyze the dynamics of the lower-atmospheric plasma.

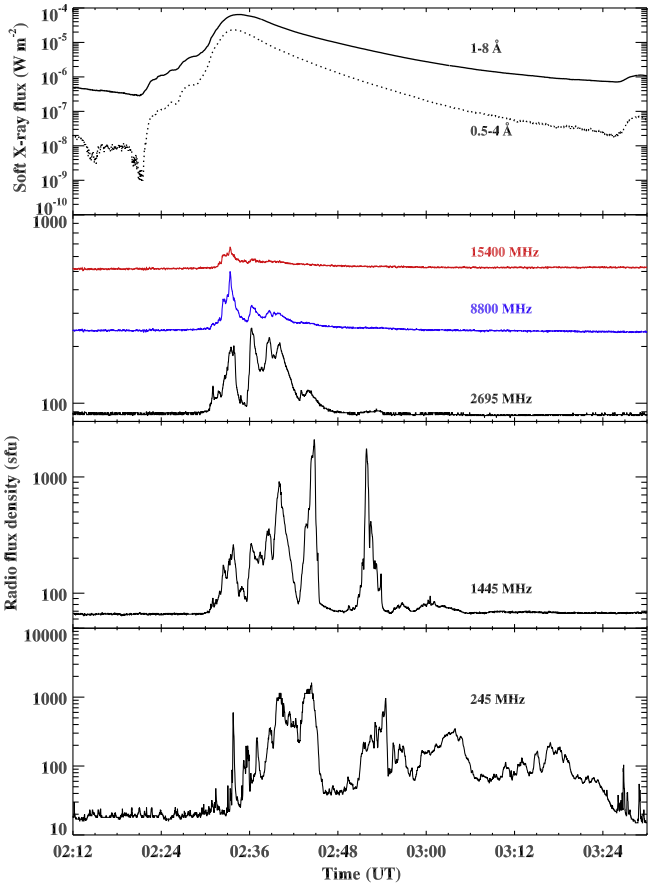

Fig. 1. Top panel: GOES soft X-ray flux profile in two different wavelength bands. Middle and Bottom Panels: RSTN 1.0 s cadence radio flux profiles in different frequencies.

Multiwavelength analysis is also important for understanding the origin of eruptions in the active regions and their connection to the various layers of the solar atmosphere. STEREO images clearly show the low-atmospheric origin of the mass eruption. It is clear in both STEREO-A and B 304 Å images that a ring-shaped mass is detached above the flare location in the field of view (cf., Figs. 2 and 3). In the STEREO-A snapshot at 02:31:15 UT, a flux-tube (loop) appeared above the flare location, which was later detached and moved up. It also expanded during its upward propagation as observed between 02:33-02:41 UT. The upward-moving front of the mass lump was clearly visible at 02:38:45 UT. The approximate lower-bound speed of the center of mass of this eruptive material was measured to be ~500 km/s in the chromosphere, which is appropriate for the upward eruption in the corona. However, the estimated speed is the lower-bound projected speed, and the actual speed of the erupting mass may be even higher in the lower solar atmosphere.

2.2. STEREO-A 171 Å and B 195 Å coronal observations

Figs. 4 and 5 show the typical sequence of EUV STEREO-A 171 Å and STEREO-B 195 Å/SECCHI images. Unfortunately, these wavelengths are not covered by both observatories simultaneously. However, both of these lines (Fe X/XI 171 Å and Fe XII 195 Å) are formed in the inner corona at temperatures between 1 and 2 MK. Therefore, they are complementary to each other in evaluating the coronal scenario of the flare and associated eruption. The NOAA

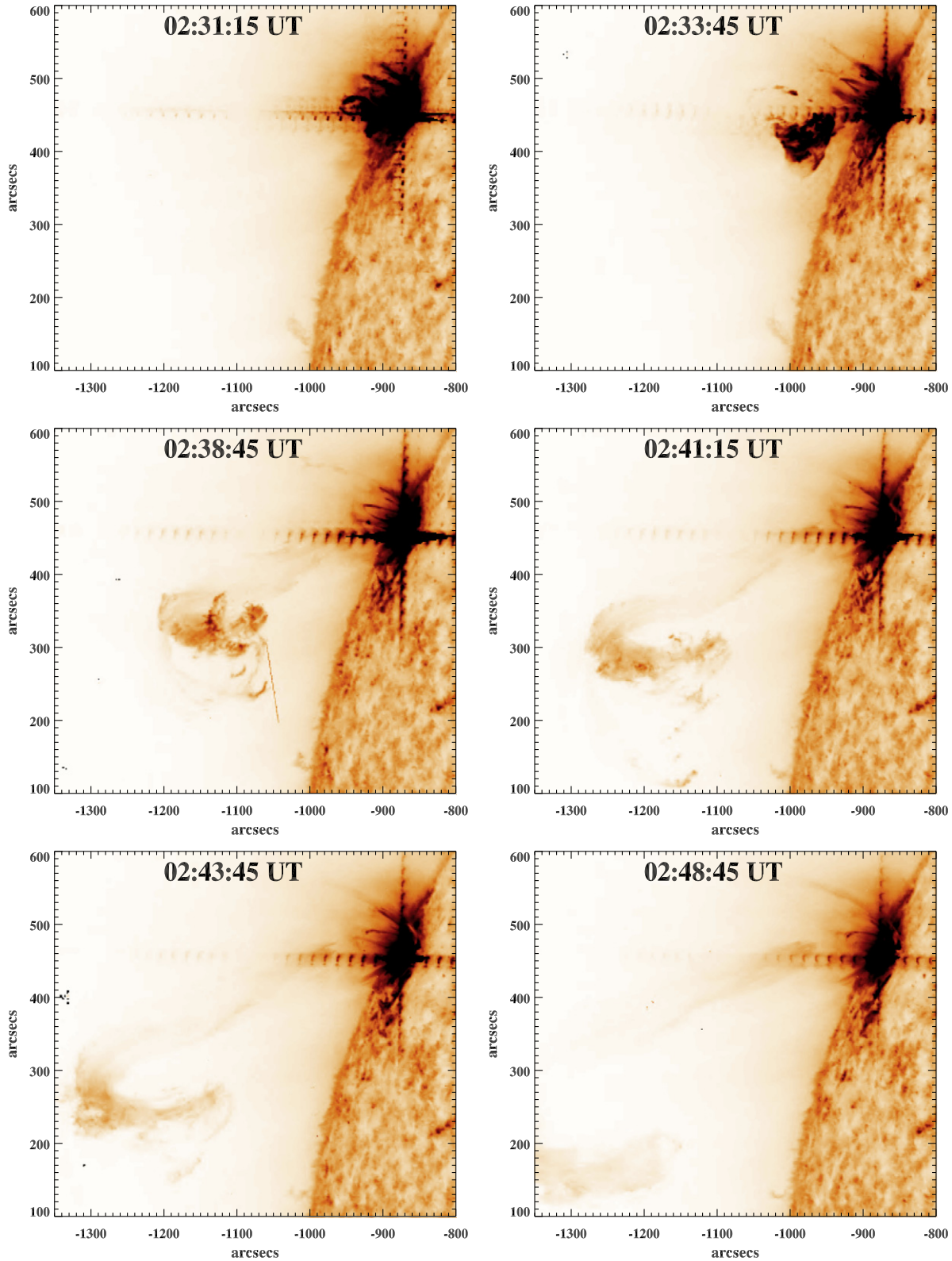

Fig. 2. STEREO-A SECCHI 304 Å EUV negative images showing the flare and associated eruption in the lower solar atmosphere.

AR 11045 was located near the northeast limb in the field of view of STEREO-A 171 Å SECCHI. However, it was observed near the northwest limb by STEREO-B 195 Å. This is due to an acute-angle separation between the two observatories during observations of AR 11045 in the corona. Therefore, observations of the same active region from different angles provide an opportunity to investigate the dynamics of the inner coronal plasma associated with this active region from different orientations.

STEREO coronal images clearly show the flaring region and the associated mass eruption from the corona. It is clear from

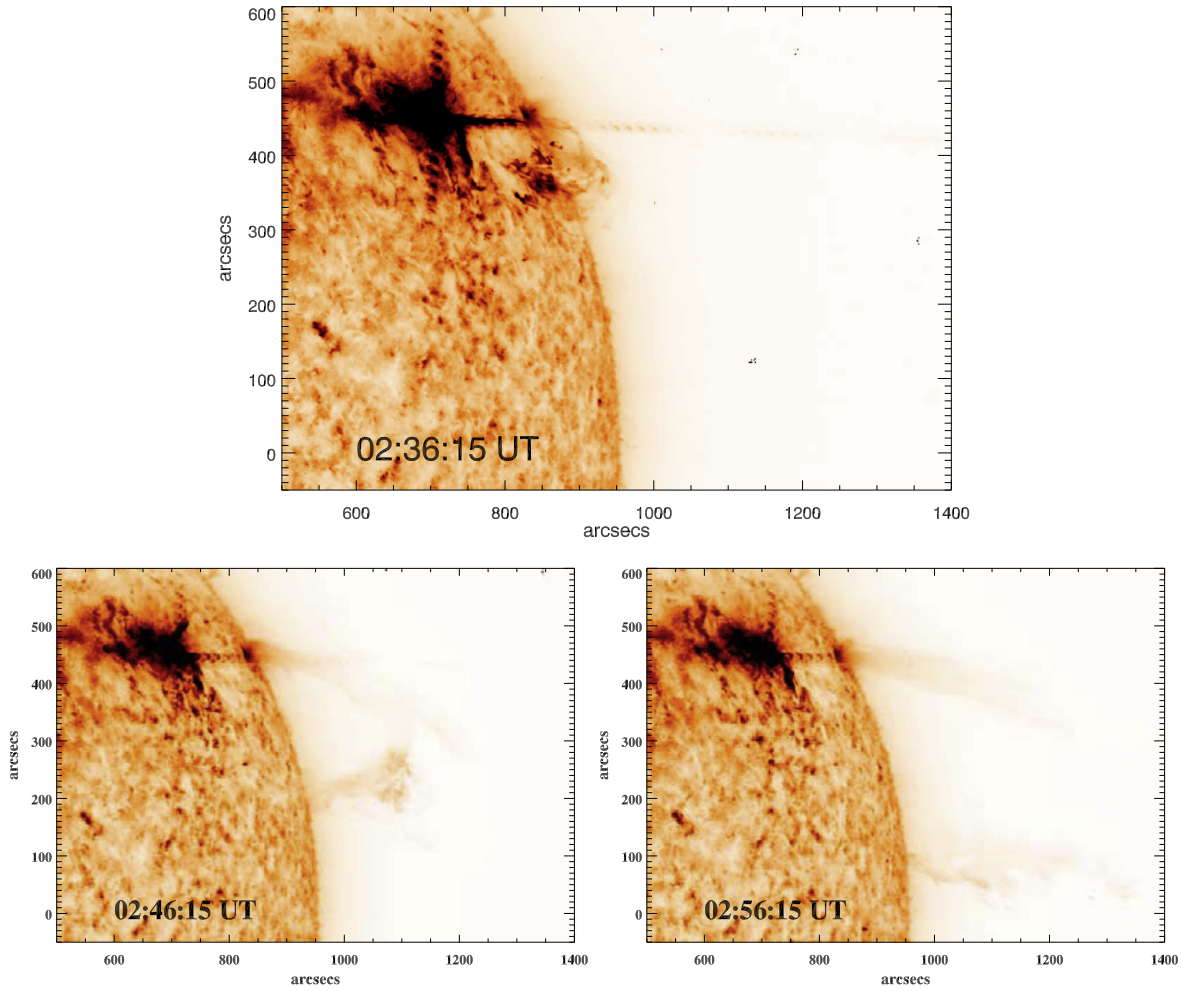

Fig. 3. STEREO-B SECCHI 304 Å EUV negative images showing the flare and associated eruption in the lower solar atmosphere from a different orientation.

STEREO-A 171 Å images that a ring-shaped mass is detached above the flare location in the field of view that is co-spatial with the STEREO-A He II 304 Å image sequence. However, it shows a higher temperature coronal part of the flaring region. In the STEREO-A snapshot at 02:32:15 UT, a loop appeared above the flare location, which later detached and moved up. It also expanded during its upward propagation as observed in the images during 02:33-02:36 UT. The upward moving front of the erupted mass is clearly visible at 02:34:45 UT. A similar situation is visible in the STEREO-A He II 304 Å image sequence. Therefore, the mass eruption has its origin in the lower atmosphere and then moves in the corona. The approximate lower-bound speed of the center of mass of this eruptive plasma is ~500 km/s in the corona, which is appropriate for an eruption towards the upper atmosphere. However, this is the lower-bound speed, and the actual speed may be higher in the solar atmosphere.

The STEREO-B 195 Å shows an interesting phenomenon, which provides an important clue to the triggering of a flare and associated mass eruption that launch a slow CME eruption in the same direction later on. At 02:20:30 UT (cf., Fig. 5), a simple bright loop was visible with a slight brightening before the initiation of the flare. However, as time progressed in the rising phase of an M-class flare (02:20 UT-02:30 UT), it was found that magnetic complexity originated in the flaring region. The two low-lying loop systems crossed each other, and an X-point was very likely formed at the flare location (02:23-02:25 UT). These loop systems reside in the low atmosphere but are visible in the coronal filters due to the filling of the hot plasma in these loops during the flaring process. These two low-lying loop systems reconnect in the lower solar atmosphere in the regime of X-type reconnection, which is evident in the snapshot at 02:28:00 UT in Fig. 5. Therefore, a ring-shaped flux tube is detached and moved upward in the higher corona. The flare triggering occurs and achieves a maximal energy-release within a few minutes after the beginning of the reconnection process. This is a typical scenario for energy release in the flaring region after the reconnection.

The SoHO/EIT 195 Å images plotted with SoHO/MDI positive- and negative-polarity magnetic field contours during different phases of the flare activity also show the formation of a quadrapolar magnetic field configuration (cf., Fig. 6). This configuration activated and generated the magnetic field complexity at the flare site itself. The magnetic field complexity is the most likely cause of flare energy build-up and its subsequent release during the reconnection process.

2.3. SOHO/MDI magnetograms and FLCT velocity maps

Using SoHO/MDI magnetograms (Figs. 7 and 8), we study the magnetic field evolution before and during the occurrence of an M-class flare and associated CME eruption. The typical size of the SoHO/MDI images is 10241024 (2″ per pixel resolution) with a cadence of 96 min (Scherrer et al., 1995). In this study, we present the partial field of view of these magnetograms, which show the evolution of the magnetic field in AR 11045. We use the standard

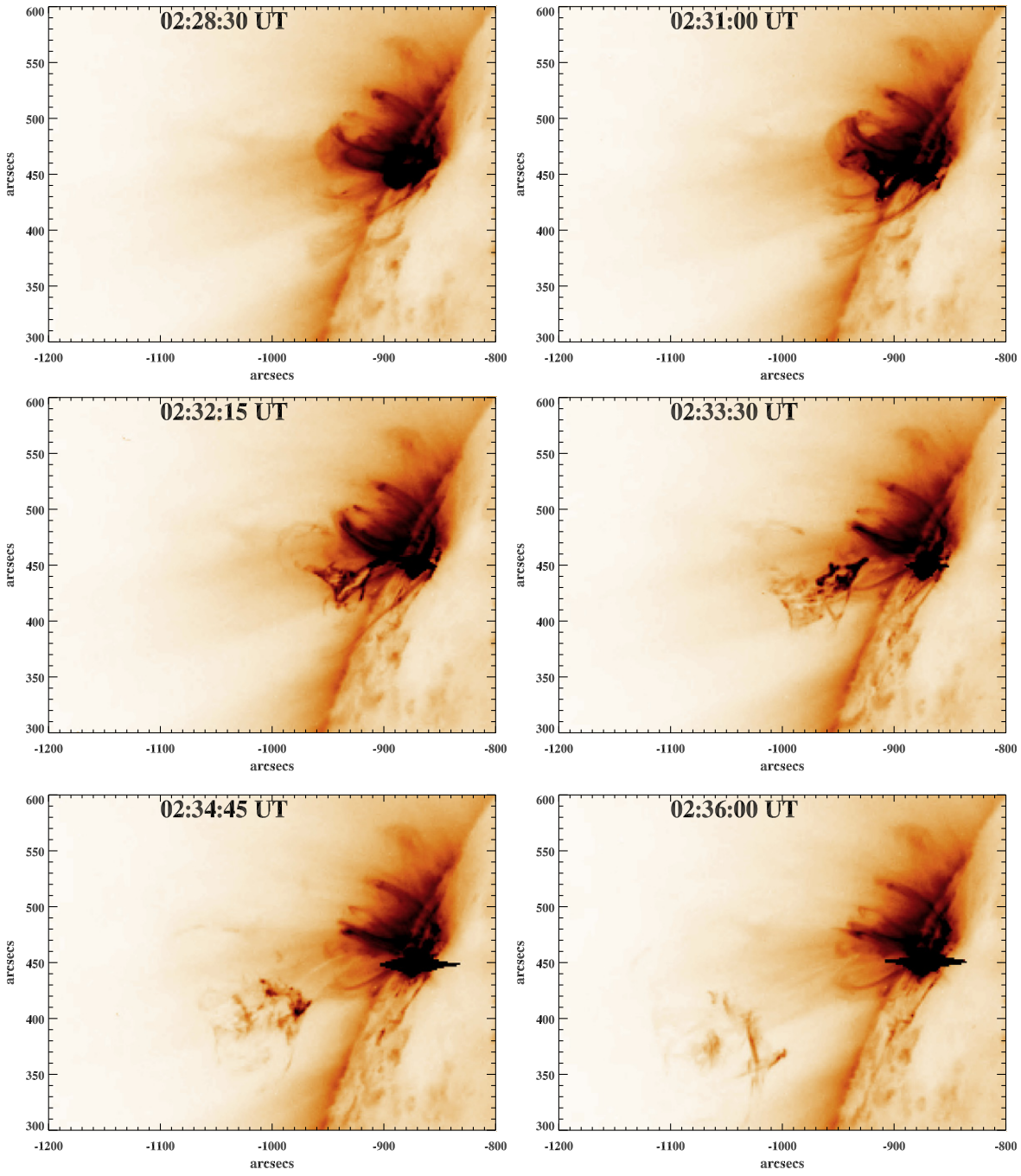

Fig. 4. STEREO-A SECCHI 171 Å EUV negative images showing the flare and associated eruption at coronal temperature.

SolarSoft library to correct the differential rotation and analyze the magnetograms. Fig. 7 displays the sequence of MDI images from February 6–7th, 2010, which reveals some interesting features of the flux emergence and the generation of magnetic field complexity in the flaring region.

The AR 11045 suddenly appeared near the northeastern limb with the evolution of weak magnetic polarities visible in the 00:03:02 UT magnetogram taken on February 6th, 2010. However, a pair of positive and negative polarity emerged within 12 h on the same day in the active region. A strong remote negative polarity also emerged on the western side of this newly emerged bipole, which moved away towards the west as time progressed. Similarly, a strong remote positive polarity also emerged on the eastern side of this newly emerged bipole at the center of the active region, moving away towards the east as time progressed. It is clear from SoHO/EIT images overplotted by MDI contours (cf., Fig. 6) that these two remote polarities are associated with higher coronal loops, which remain static and stable in the active region and do not show any significant topological changes before or after the flare and CME eruption (cf., Fig. 6). The western remote negative polarity also joined in the formation of a small coronal loop system with some positive polarities lying in the southward direction of the active region near the flare site. However, the energy build-up, its release, and mass eruption are caused by an emergence of magnetic field polarities, their motion, as well as generation of magnetic field complexity at the center of the active region between the emerged remote bipole (cf., Fig. 7). At 12:47:02 UT on 6 February 2010, the emerged negative polarity pushed its positive

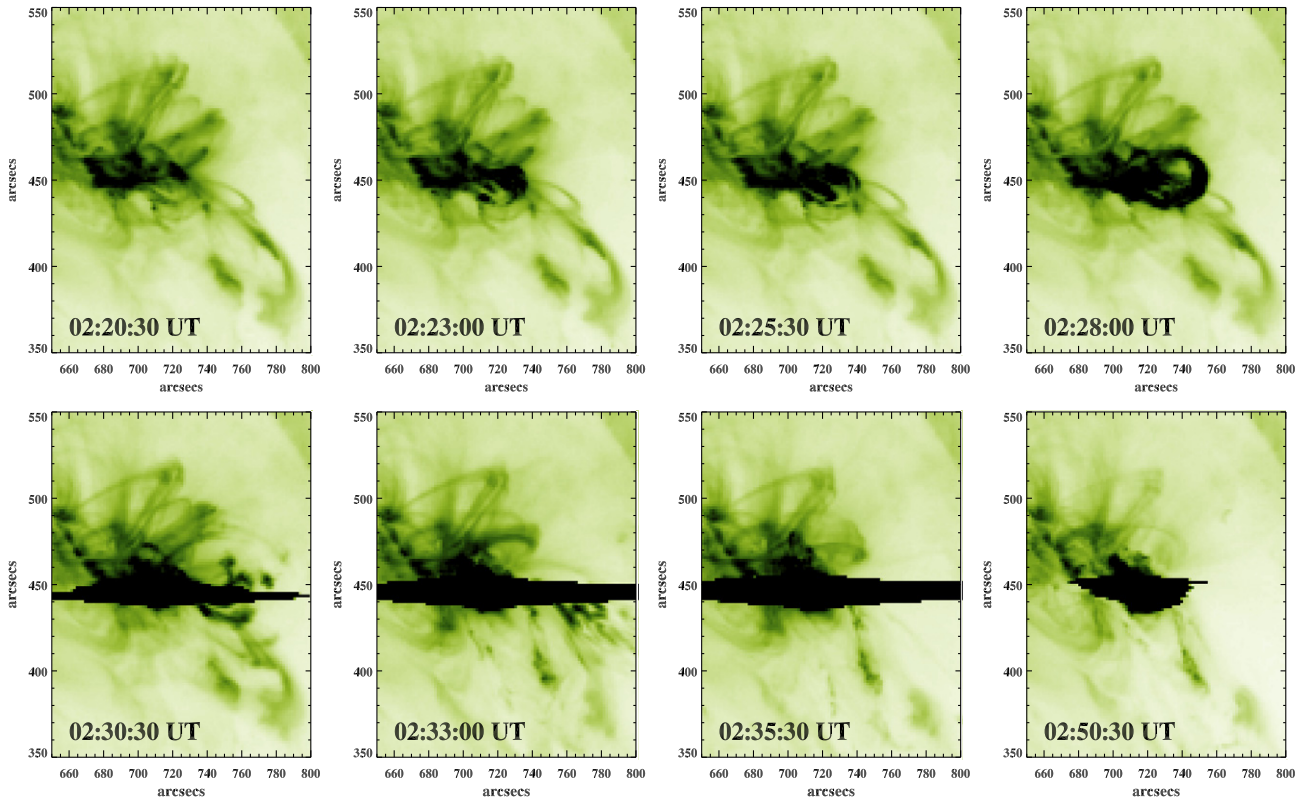

Fig. 5. STEREO-B SECCHI 195 Å EUV negative images showing the flare and associated eruption at coronal temperature.

counterpart without showing any signs of magnetic field cancellation. At 20:47:02 UT on the same day, it penetrated and divided the positive polarity into two parts. This penetration continued into the next day (February 7th, 2010), accompanied by additional emergences of positive and negative polarities during an M-class flare and related eruption.

To confirm this motion, which is crucial to understand the flare energy build-up, we measured the photospheric horizontal flow pattern in and around the emerging bipole in the active region at the flare site using the Fourier Local Correlation Tracking Technique (FLCT) on SoHO/MDI images. The FLCT method is described by Welsch et al. (2007) and Fisher and Welsch (2008). The main input parameters for this technique are two images, f1 and f2, the pixel separation scale (s), time separation (t) scale, and a Gaussian window size scale (σ). This routine calculates the velocity (two-dimensional) by maximizing the cross-correlation of each image when weighted by the Gaussian window centered on each pixel location. In our study, we used the two SoHO/MDI frames at different times before the flare. After a careful investigation, a Gaussian window with a standard deviation of 15″ was chosen. Fig. 9 displays the photospheric velocity map obtained by the FLCT technique using SoHO/MDI magnetograms. The longest arrow corresponds to a velocity of 0.30 km/s. It may be noted from the flow map on February 6th, 2010 that the photospheric flow was mostly streamlined from the east to westward direction in the area of the emerged bipolar region at the flare site between two large, remote bipolar areas of the active region. Later, the flow pattern became complex and chaotic around the emerged bipole at the flare site when its negative polarity region penetrated and divided its positive counterpart into two parts. We do not find any signature of a magnetic flux cancellation during this process. The change of configuration was most likely related to complex photospheric flows that showed opposite vortices around the pair of opposite-polarity spots at the flare site primarily in the central part of this active region. The negative-polarity spot, which rotated counterclockwise, broke the positive-polarity spot into two regions. The bi-halved positive polarity rotated in the clockwise direction. This unique physical scenario eventually led to the build-up of the flare energy.

Another interesting scenario is evident in the SoHO/MDI and FLCT flow-velocity maps. It is clear that a pair of positive and negative polarities also emerged in the eastern side of the negative polarity of the flare site and in the western side of the remote eastern positive polarity. It is also evident in the MDI images from February 7th, 2010 that before and after the flare, this emerged-positive polarity exhibited a shape reversal (cf., 01:39 UT and 03:15 UT snapshots in Fig. 7). This was most likely due to the rotation of the associated minor spot and thus the build-up of magnetic field complexity, which also occurred in the eastern side of the flaring region (e.g., Kumar et al., 2011 and references cited there). When the main negative polarity penetrates and divides the positive polarity into two parts at the flare site, magnetic complexity is generated. The simple bipolar configuration of the magnetic field at the flare site is likely disturbed and becomes more intricate. As a result, a more complex quadrapolar magnetic field configuration is generated.

It is also clear from the coronal images that the simple bipolar loop system is combined into the quadrapolar, low-lying loop system that cross each other (cf., 02:20-02:28 UT snapshots in STEREO-B 195 Å). These two loop systems crossed each other and probably reconnected at an X-point formed in the lower solar atmosphere under a quadrapolar magnetic field configuration. The upper-lying loop system seems to be detached during this ongoing reconnection process and during the triggering and eruption of an M-class flare in the upper solar atmosphere (cf., 02:30 UT-02:35 UT snapshots of STEREO-B 195 Å). This detached flux tube expanded, and, in association with the flare activity, the origins of a slow CME occurred. This is not a typical CME but an

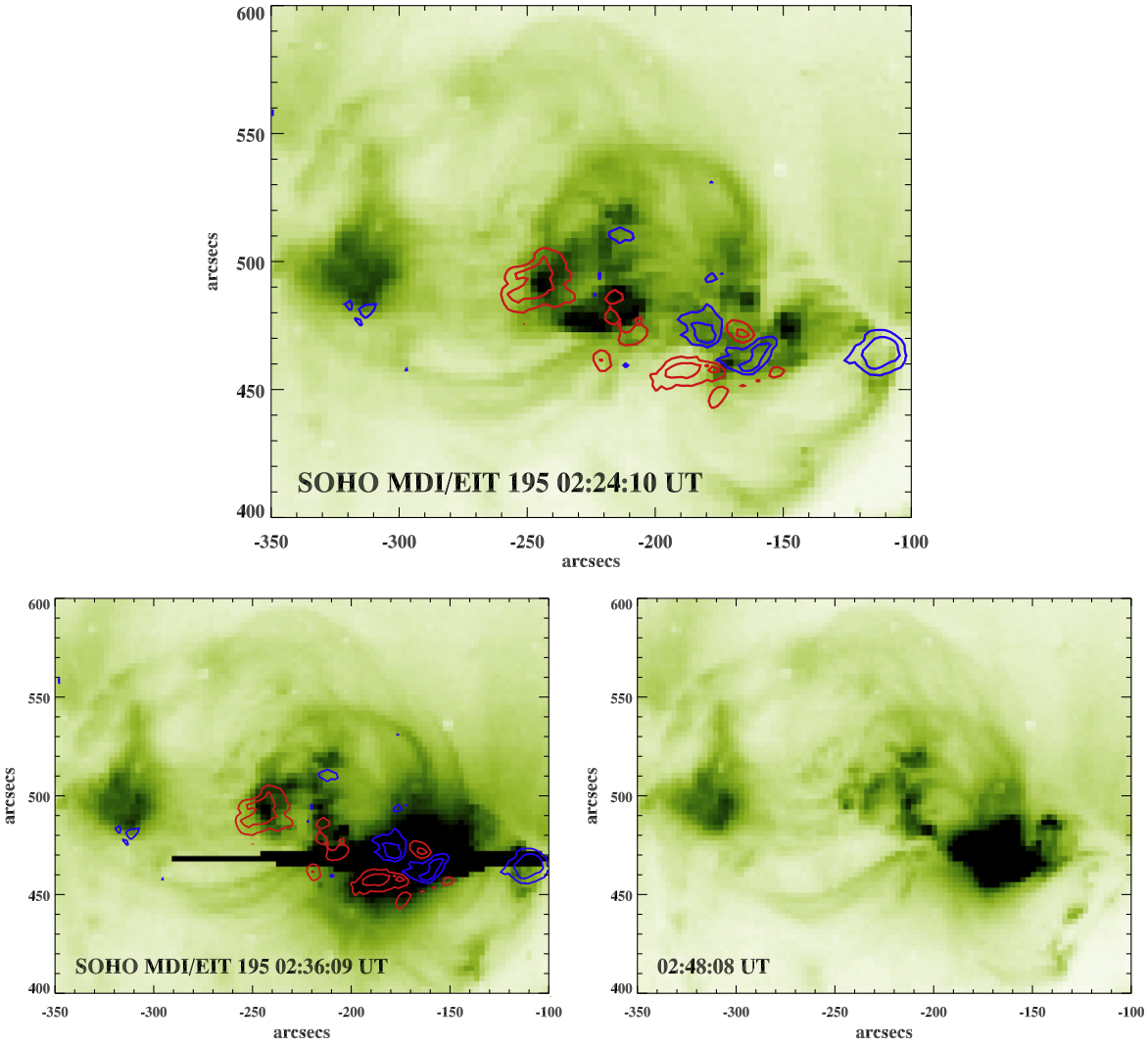

Fig. 6. EIT 195 Å EUV negative images overlaid by SOHO/MDI contours (Red = +ve, Blue = −ve). (For interpretation of the references to colour in this figure legend, the reader is referred to the web version of this article.)

expansion of the detached flux tube during the flare process. According to the LASCO CME catalog (cf., http://cdaw.gsfc.nasa.gov/), we find that this halo CME reached the field of view of C2-coronagraph on 03:54 UT in the same direction above the observed flaring active region with a speed of 421 km/s, angular width of 360°, and a slow acceleration of 0.5 m/s^2. However, according to the CACTUS CME Catalog (http://sidc.oma.be/cactus/catalog.php), this CME was found to move with a maximum speed of 446 km/s. Its traces may also be evident in the outer corona during the peak of the flare in AR 11045. The CME launch time at one solar radius approximately matches the flare duration and the detachment of the ring-shaped flux tube in the lower solar atmosphere. Fig. 9 shows 17-GHz radio emissions at the flare site that confirm the reconnection event in the lower solar atmosphere at the flare site. It also provides evidence of the acceleration of non-thermal particles in the associated loop system that generate the 17 GHz radio emissions in the lower solar atmosphere.

Tanaka (1991) and Kurokawa et al. (2002) have found observational evidence of the evolution of sunspot groups, their rotation and collision, as well as their disappearance in flaring active regions. They have concluded that the complex evolution of the spot groups in the rapidly emerging active regions may lead to the emergence of twisted and sheared flux tubes and the generation of an associated magnetic field complexity. In the present work, we also find evidence of dipolar-field configuration changes to the more complex quadrapolar magnetic fields, as well as the signature of flux emergence in and around the flaring site. We also find the response of these changes at the photosphere in the corona where the overlying-loop systems' magnetic fields become more complex and reconnect for the flare energy release and associated eruption (cf., cartoon description in Fig. 10). Our results provide a comprehensive morphological view of the AR 11045 dynamics occurring on February 7th, 2010 and the associated M-class flare and eruptions from the photosphere to the corona using multiwavelength observations from various space- and ground-based observatories.

3. Discussion and conclusion

In this paper, we study the multiwavelength observations of an M6.4 flare and associated eruptions in Active Region NOAA 11045 on February 7th, 2010. The space- and ground-based observations from STEREO, SoHO/MDI, EIT, and Nobeyama Radioheliograph are used for the study. This active region rapidly appeared at the northeastern limb with an unusual magnetic field emergence.

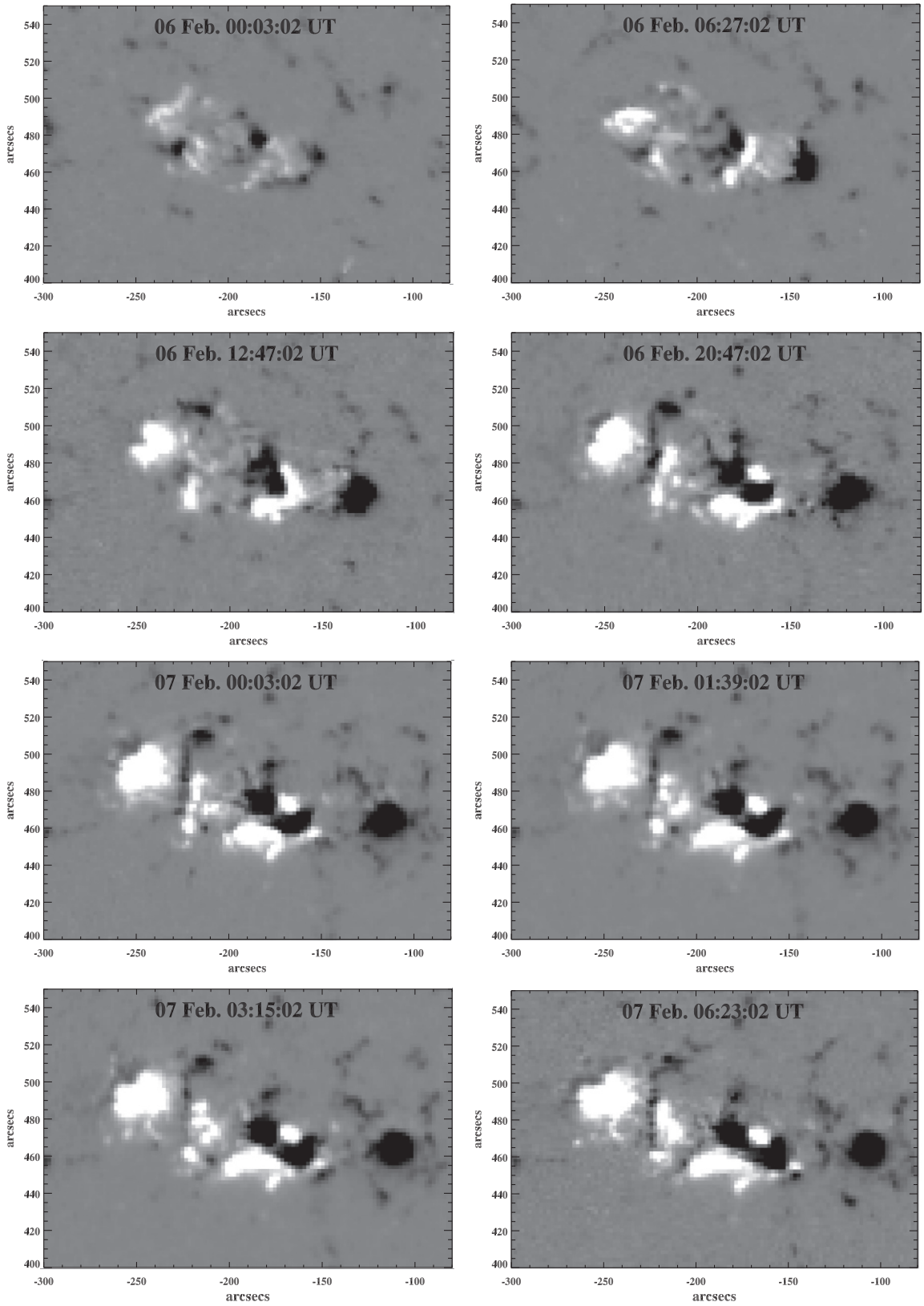

Fig. 7. SOHO/MDI magnetograms showing rapid flux emergence in the active region.

We find a unique observational signature of the magnetic field configuration at the flare site changing from a dipolar to quadrapolar topology. This change in the magnetic field configuration results in a complex magnetic field structure and a build-up of the flare energy. The M-class flare was most likely triggered due to magnetic reconnection in the quadrapolar regime where two low-lying loop systems reconnected with each other. It should be noted that the formation of an X-reconnection point in the lower solar

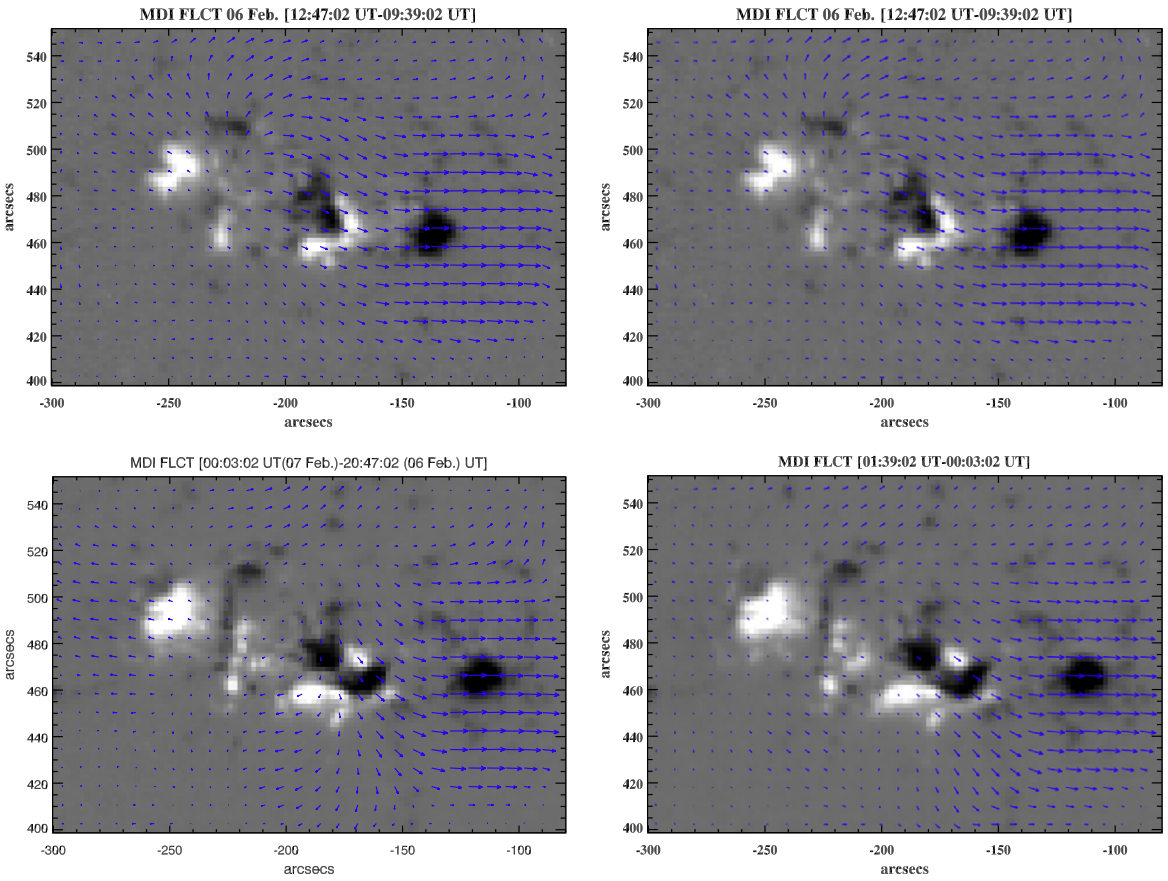

Fig. 8. FLCT velocity map of the active region. The longest arrows (left and right) correspond to the flow velocities of ∼0.128 and ∼0.300 km/s, respectively.

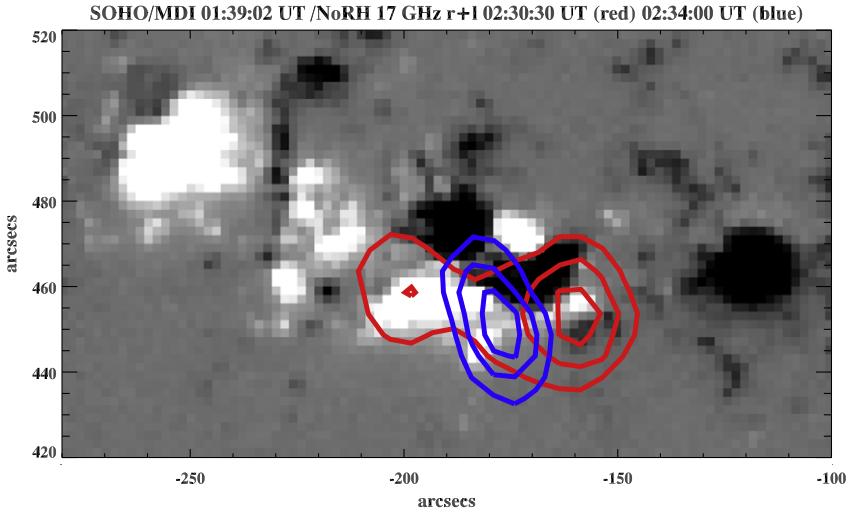

Fig. 9. NoRH 17 GHz image contours overlaid on a SOHO/MDI image of the active region. The contour levels are 50%, 70%, and 90% of the maximum intensity. The footpoints (red) and looptop (blue) sources are evident during the flare. (For interpretation of the references to colour in this figure legend, the reader is referred to the web version of this article.)

atmosphere probably lies in the chromosphere. We did not find any signature of magnetic flux cancellation during this process. We interpret the change in the magnetic field configuration as a consequence of the flux emergence and photospheric flows that have opposite vortices around the pair of opposite-polarity spots. The negative-polarity spot rotating counterclockwise breaks the clockwise-rotating positive-polarity spot into two parts. The STEREO-A 195 Å and STEREO-B 171 Å coronal images during the flare reveal that a twisted flux tube expands and erupts resulting in a slow coronal mass ejection. The formation of co-spatial bipolar radio contours at the same location also reveals the ongoing reconnection process above the flare site and thus the acceleration of non-thermal particles.

The reconnection may also be responsible for the detachment of a ring-shaped twisted flux tube that further causes a halo CME eruption with a speed of 446 km/s in the outer corona. The

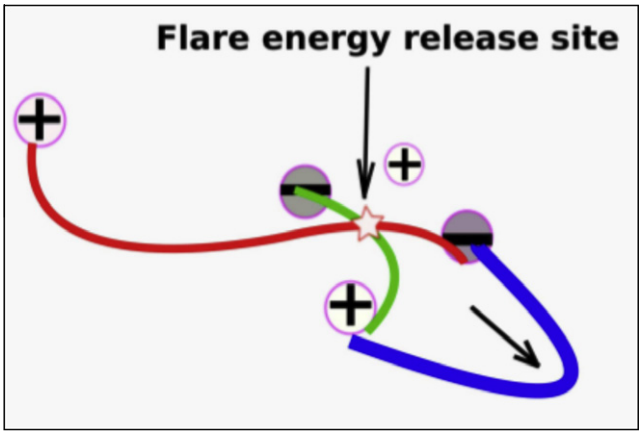

Fig. 10. The schematic diagram that shows the reconnection of the low-lying loop systems, flare energy release, and associated eruption.

reconnection by the two low-lying loop systems in the lower solar atmosphere and the detachment of the overlying-supersonic flux tube towards the outer corona generate a slow CME associated with the flare. Therefore, our observations may provide a very rare case study for the flare-CME relationship. However, in the present paper, we aim to study only the triggering of the M-class flare and associated eruption in the lower atmosphere at the flare energy build-up site. The lump of mass erupted above this reconnection point with an upward speed of ~500 km/s from the lower solar atmosphere. This mass eruption was also visible in the coronal lines with approximately the same speed. The mass later expands into the upper corona and is associated with a halo CME propagating in the outer corona with a speed of ~446 km/s. We do not aim to study the propagation properties of the CME in the outer corona as it was in the opposite direction to the Earth without any space weather consequences. However, we aim to understand the initiation mechanisms of such CMEs associated with flares, which may affect the heliospheric environment.

In conclusion, we described multiwavelength observations of the triggering of an M-class flare in terms of the magnetic complexity during the strong emergence of magnetic polarities in AR11045. We find that the mass eruption and flare energy release were due to quadrapolar X-type magnetic reconnection in the lower solar atmosphere. Our observations describe the initial triggering mechanism of a halo CME associated with the solar flare. However, future multiwavelength high spatio-temporal observations should be carried out at recently developed space-based (SDO, Hinode, STEREO) and ground-based (SST, DOT, ROSA) observatories to arrive at a more definite conclusion about the initiation mechanisms of the solar flares and associated CMEs.

Acknowledgments

We thank the reviewer for his/her valuable suggestions that improved our manuscript considerably. Hinode is a Japanese mission developed and launched by ISAS/JAXA with NAOJ as a domestic partner and NASA and STFC (UK) as international partners. It is operated by these agencies in co-operation with ESA and NSC (Norway). We also acknowledge the SoHO/MDI, EIT, STEREO, and Nobeyama Radio observations used in the paper. AKS acknowledges the joint DST-RFBR (INT/RFBR/P-38) project for the present research and also thanks Shobhna Srivastava for patient encouragement during the work.

Note added in proof

We came across the paper by L.P. Li, J. Zhang, T. Li, S.H. Yang, Y.Z. Zhang Li (2012) (cf., http://dx.doi.org/10.1051/0004-6361/201015796; A&A; Accepted 9 December 2011) have also studied statistically the first flare productive active region AR 11045 of the current solar cycle 24 and explained the case study of filament eruption and solar flare on 7 February 2010. However, we have studied in detail at multiwavelength the connection of the flare and related mass eruption with the photospheric magnetic field activity (cf., http://dx.doi.org/10.1016/j.newast.2011.10.004; Accepted 19 October 2011).

References

Foullon, C., Verwichte, E., Nakariakov, V.M., Nykyri, K., Farrugia, C.J., 2011. ApJ 729, L8.
Cho, K.S., Lee, J., Bong, Kim, Y., Joshi, B., Park, Y., 2009. ApJ 703, 1.
Fisher, G.H., Welsch, B.T., 2008. ASPC 383, 373.
Jain, R., Aggarwal, M., Kulkarni, A., 2010. RAA 10, 473.
Kumar, P., Manoharan, P.K., Uddin, W., 2010a. ApJ 710, 1195.
Kumar, P., Srivastava, A.K., Filippov, B., Uddin, W., 2010b. Sol. Phys. 266, 39.
Kumar, P., Srivastava, A.K., Somov, B.V., Manoharan, P.K., Erdélyi, R., Uddin, W., 2010c. ApJ 723, 1651.
Kumar, P., Srivastava, A.K., Filippov, B., Erdélyi, R., Uddin, W., 2011. Sol. Phys. 272, 301.
Kurokawa, H., Wang, T., Ishii, T.T., 2002. ApJ 572, 598.
Liu, R., Gilbert, H.R., Alexander, D., Su, Y., 2008. ApJ 680, 1508.
Scherrer, P.H., Bogart, R.S., Bush, R.I., et al., 1995. Sol. Phys. 162, 129.
Shen, Y., Liu, Y., Liu, R., 2011. RAA 11, 594.
Srivastava, A.K., Zaqarashvili, T.V., Kumar, Pankaj, Khodachenko, M.L., 2010. ApJ 715, 292.
Tanaka, K., 1991. Sol. Phys. 136, 133.
Welsch, B.T., Abbett, W.P., De Rosa, M.L., Fisher, G.H., Georgoulis, M.K., Kusano, K., Longcope, D.W., Ravindra, B., Schuck, P.W., 2007. ApJ 670, 1434.
Xu, Y., Liu, R., Jing, J., Wang, H., 2010. Amer. Astron. Soc. Meet. 216, 404.